https://doi.org/10.1016/j.jallcom.2018.06.042

Efficient fabrication of gradient nanostructure layer on surface of commercial pure copper by coupling electric pulse and ultrasonics treatment

Renjie Ji [a,b,*], Yonghong Liu [a], Suet To [b,**], Hui Jin [a], Wai Sze Yip [b], Zelin Yang [a], Chao Zheng [a], Baoping Cai [a]

[a] *College of Mechanical and Electronic Engineering, China University of Petroleum (East China), Qingdao, Shandong, 266580, PR China*

[b] *State Key Laboratory in Ultra-precision Machining Technology, Department of Industrial and Systems Engineering, The Hong Kong Polytechnic University, Hong Kong, China*

[*] Corresponding author. College of Mechanical and Electronic Engineering, China University of Petroleum (East China), Qingdao, Shandong, 266580, PR China.

** Corresponding author.

E-mail addresses: jirenjie@upc.edu.cn (R. Ji), sandy.to@polyu.edu.hk (S. To).

Efficient fabrication of gradient nanostructure layer on surface of commercial pure copper by coupling electric pulse and ultrasonics treatment

Severe plastic deformation can be easily produced on metal surfaces by coupling the micro thermal shock from high peak pulse current and the micro mechanical shock from ultrasonics. Moreover, an efficient method for preparing a gradient nanostructured metal surface by coupling electric pulse and ultrasonics treatment (CEPUT) is developed in this study. The variation in microstructure and hardness of the specimen are investigated by electron backscatter diffraction, transmission electron microscope, X-ray diffraction, and nano-indentation measurement. Results showed that on the treated copper surface with CEPUT, the original grain boundaries are no longer recognized, the average grain size decreases from 48.77 μm to 39.22 nm, and the thickness of severe plastic deformation layer reaches to approximately 500 μm. Moreover, the hardness reaches to 2.105 GPa, and CEPUT also reduces the texture in the sample surface. A computational model is developed and the grain refinement mechanism is proposed to describe the electrical-thermal-mechanical phenomena during CEPUT. The proposed simple and costeffective method of grain refinement and to produce the graded materials is effective, especially in the materials of high thermal and electrical conductivity.

Keywords: Coupling electric pulse and ultrasonics; Severe plastic deformation; Grain boundaries; Gradient nanostructure layer; Transmission electron microscopy

Subject classification codes:

Introduction

Metallic materials with nanometer grain size (average < 100 nm) in the top surface have attracted intensive research due to their superior physical and mechanical properties and improved service life [1-6]. The metallic materials' nanostructure surface is important for increasing their service life because many failures originate at or near the materials' surface. In recent years, mechanical treatment methods, such as high energy shot peening [7], supersonic fine particles bombarding [8], surface mechanical attrition treatment (SMAT) [9], high-pressure torsion [10], platen friction sliding deformation [11], have gradually attracted significant interest from researchers. On the basis of the above-mentioned methods, severe plastic deformation (SPD) and a lot of crystal defects have easily occurred in the metal surface in which the surface grain size is reduced to nanoscale and the gradient nanostructure (GN) layer is generated at the metal surface. Moreover, the adhesion force between the nanocrystalline surface layer and metal matrix is good. Furthermore, low plasticity burnishing [12] and water jet cavitation peening [13] are common technologies that cause SPD at the surface region to generate a GN surface layer on metallic materials. Thus, these technologies have attracted considerable attention recently. Ultrasonic vibration energy could significantly soften the metallic materials without significant heating, which is usually termed as acoustoplastic or acoustic softening effect. From its first observation, ultrasonic vibration energy has been widely used to assist the plastic deformation and improve the material flow in metal processing using SPD methods [14-16]. Liu et al. [17] applied ultrasonic waves on a plastic deformation area during its conventional upsetting to refine material grains. Their experiment and simulation results showed that the produced stress by ultrasonic vibrations increased the plastic deformation. Djavanroodi et al. [18] investigated the effect of ultrasonic vibrations on the deformation behavior of pure commercial aluminum in the equal channel angular pressing process. They determined that the forming force decreased with the increase of vibration amplitude and vibration frequency. Moreover, ultrasonic assisted equal channel angular extrusion [19], ultrasonic impact treatment [20,21], ultrasonic surface rolling process [22], and ultrasonic nanocrystal surface modification [23] were investigated, and the results indicated that ultrasonic vibrations induced SPD and improved the grain refinement efficiency in SPD processes. Laser shock processing (LSP) is a surface treatment technology, and the mechanical effect of a laser shock wave with highinstantaneous-energy-density induces high compressive residual stress and microstructural evolution that generate nanocrystal grains on the metal surface [24,25]. However, a confined medium and a coating layer required on the metal surface during LSP complicate the process. The electroplastic effect induced by a high-density pulse current in metals was discovered in the 1960s, and its mechanism has been investigated for decades [26-28]. Moreover, the electroplastic effect can decrease the flow stress, improve the deformation limit of metallic materials, and enhance the mobility of dislocations, atomic diffusion and vacancy diffusion. Thus, the electroplastic effect has been recognized due to its high efficiency and has attracted extensive studies in materials science and engineering, such as rolling, drawing, and refining grain [29-33]. On the basis of the above mentioned grain refinement methods, SPD were caused by either the applied loads, the instantaneous heat, or the electroplastic effect, and grain refinement methods experienced low processing efficiencies that hindered the widespread application of surface nanocrystallization methods. In this study, we find that SPD is easily produced and significantly enhanced on metal surfaces by coupling the micro thermal shock from high peak pulse current and the micro mechanical shock from ultrasonics. Moreover, an efficient method for preparing a GN metal surface by coupling electric pulse and ultrasonics treatment (CEPUT) is developed, and the preparation mechanism and the physical characteristics of a GN layer are investigated. The rest of the paper is structured as follows: Section 2 describes the principle, experimental details, and numerical simulation of CEPUT, and the structural characterization and nano-indentation test of the sample after CEPUT. Section 3 illustrates the microstructure of the copper sample after CEPUT and the grain refinement process, and analyzes the performance of the treated copper sample to provide insight on the mechanism and advantage of the CEPUT method. Section 4 provides the conclusion.

Material and Method

Principle of CEPUT

The physical model and experimental device for CEPUT are shown in Fig. 1. As depicted in Fig. 1A, the heat from electric pulse and the force from ultrasonic vibration both act on the sample surface by tool impacting. The electric current transiently increases during the electric pulse (Fig. 1B), and the contact resistance is high at the contact point. Thus, the temperature rapidly increases at the contact point. The electric current duration is very short, the electric current rapidly decreases, and the working fluid is flushed to the contact point between the tool and the sample with a nozzle at room temperature. Thus, the temperature at the contact point rapidly decreases, and the high temperature gradient and the high thermal stress are obtained during CEPUT. High equivalent stresses are generated at the contact point coupled with continuous ultrasonic shocks. Meanwhile, the high peak pulse current (Fig. 1B) at the contact point makes the electron within the material rapidly move along the electric field, and the produced large electronwind-force assists the dislocation motion and opens the tangles of dislocations due to the electroplastic effect [34,35]. Thus, the deformation resistance significantly decreases, the plasticity is significantly enhanced, and SPD easily occurs that contribute in grain refinement to produce a nanocrystalline layer on the metal surface. In this study, the mechanical force is composed of the preload pressure from air and the ultrasonic vibration impact force from the tool, the heat is generated by the high-instantaneousenergy-density pulse current during CEPUT, and the developed experimental device for CEPUT is depicted in Fig. 1C. As shown in Fig. 1C, the experimental sample rotates at velocity V1, and the treatment tool is forced on the sample surface and slides along the sample axial direction at velocity V2. The treatment tool and the sample are connected to the positive and negative poles of the electric pulse generator, respectively. The working fluid is flushed to the contact point between the tool and the sample with a nozzle at room temperature. The sample surface is treated by one pass when the tool tip slides from one end of the sample to the other end. After several passes of treatment, the sample surface grain is sufficiently refined, and the compact nanocrystalline layer is produced on the metal surface. Moreover, the electric current is generated during CEPUT, and the produced heat should be dissipated rapidly to prevent the sample surface from hurting Thus, good thermal and electrical conductivity of the sample material are required.

Experimental Detail for CEPUT

In this study, a commercial purity copper was used as an example to demonstrate the capability of the technique as well as the structure and properties of the CEPUT processed sample. Copper was annealed at 823 K for 3 h to obtain a polycrystalline structure. The average grain diameter of the as-annealed sample was 48.77 µm (Fig. 2). The X-ray diffraction (XRD) pattern of the copper sample is shown in Fig. 3. The diameter of the copper sample was 30 mm. The ultrasonic vibration tool with a hemispherical tip was an MG18 cemented carbide cylinder with a diameter of 6 mm. On the basis of the previous experimental research, treatment with 10e15 passes was sufficient to produce the nanocrystalline layer on the sample surface, and the workpiece was treated by 12 passes in this study. During the treatment, the static force was set to 600 N to maintain a good contact between the ultrasonic vibration tool and the workpiece, V1 was 250 rpm, V2 was 5 mm/min, the ultrasonics frequency was 26 kHz, the ultrasonics amplitude was 10 µm, the power output of the ultrasonics generator was 500 W, the peak current of electric pulse was 1000 A, and the electric pulse frequency was 1000 Hz. Thus, the feed rate per revolution and the number of strikes per mm^2 were calculated as 0.02 mm and 3.3 103 , respectively. Moreover, the cooling water was flushed to the contact point using a self-priming pump (HL3208, Hua Lei TeElectrical co., Ltd., China), the water flux was 4 L/ min.

Structural characterization and nano-indentation test of the sample after CEPUT

The electron backscatter diffraction (EBSD) analysis on the treated workpiece section was conducted by using a thermal field emission scanning electron microscope (JEOL JSM-7001 F, JEOL Ltd.), equipped with an EBSD analysis apparatus (TSL Incorporated, USA). It is important to note that during the EBSD analysis on the untreated copper sample, the scanning step was set to 1.10 μm to reduce computation time, and the resolution ratio was insufficient. Thus, most of the grain boundaries were corrugated and indicated saw tooth morphology, as shown in Fig. 2. Structural characterization and gain size of the treated workpiece surface were performed by an XRD (X' Pert PRO MPD) with a CuKa radiation and a transmission electron microscope (TEM, TECNAI G2 F20 S-TWIN) under a voltage of 200 kV. The accelerating voltage and the applied current for XRD were 40 kV and 40 mA, respectively. The sample for TEM observation was prepared by a focused ion beam (FIB, Helios Nanolab 600i). To investigate the variation on mechanical performance from surface to matrix, the nano-indentation measurement was performed on the sections perpendicular to the treated surface. The distance of the test points from the treated workpiece top surface are shown in Table 1. All the nano-indentation measurements in the present work were performed using a nanoindenter (G200, Agilent Technologies, USA) with a displacement resolution of 0.01 nm and a loading resolution of 50 nN. This instrument was equipped with a standard Berkovich indenter whose total displacement range was 2 mm. The maximum testing load was 150 mN, and the holding time corresponding to this maximum load was 30 s. In addition, the loading rate and unloading rate were both

10 mN/s. For each test condition, the procedure was repeated five times in different positions and the average value was adopted.

Numerical simulation of CEPUT

A computational model based upon finite element ANSYS software was developed to describe the electrical-thermal-mechanical phenomena of the CEPUT process. The assumed conditions for the model were expressed as follows [36]: (1) The treatment tool and the workpiece were homogenous and isotropous. (2) The treatment tool and the workpiece maintained the point contact without separation. Considering the axisymmetric geometry and loading of the treatment tool and the workpiece, the treatment tool and the workpiece were modeled by utilizing a 2D axisymmetric model, as shown in Fig. 4. As shown in Fig. 4, the eight-node plane PLANE233 element with four degrees of freedom was used to model the treatment tool and workpiece. The finite element grid in Fig. 4 had 1008 elements and 1116 nodes. Moreover, the grid was graded from fine to coarse based on the expected reduction in temperature and stress gradient when it moved away from the contact point. The boundary conditions in the calculation were expressed as follows [37,38]: (1) The electrical current was uniformly applied on the top of the treatment tool. (2) Considering that the treatment tool and the workpiece were cooled by water during CEPUT, the transferred heat to the surrounding water was obtained by heat conduction and the conductive heat transfer coefficient was 1200 W/m^2 °C. (3) The far end of the workpiece was assumed to be at ambient temperature (22 °C), which was also the initial condition. (4) The workpiece displacement was set to zero.

During CEPUT, the loads were composed of two parts. In the first part, the peak electric pulse current was 1000 A, the pulse width was 4 x 10^{-5} s, and the pulse interval was 9.6 x 10^{-4} s, as shown in Fig. 1B. The current that flowed from the upper treatment tool and zero potential was applied on the workpiece surface. Meanwhile, a sine wave force was applied on the upper treatment tool to simulate the ultrasonic shock. Several essential property parameters of the workpiece and the treatment tool used in the model were listed in Table 2. The simulation procedure of CEPUT process was shown in Fig. 5.

Result and Discussion

Fig. 6 provides an overview on the microstructural observations of the copper sample after CEPUT based on TEM, EBSD and XRD examination. Fig. 6A shows the microstructural transition from nanostructured surface to deformed grains in the top 700 µm of the sample, in which the black dashed line indicates the treated surface. As shown in Fig. 6A, a clear microstructural gradient is developed after CEPUT. A large amount of plastic deformation is introduced in the top to about 500 µm, where the original grain boundaries are no longer recognized. The microstructural morphology considerably varies in a continuous manner with depth from the treated surface, which is analogous on the microstructure evolution as a time function for the CEPUT process. Fig. 6B shows the TEM bright field image, and the corresponding selected area electron diffraction (SAED) pattern, and Fig. 6F shows the XRD pattern of the treated workpiece top surface indicated in Fig. 6A. The nanoscale microstructure, which is mostly non-indexed in EBSD maps due to

SPD after CEPUT, is characterized by TEM at the treated top surface. Moreover, the grains are uniform and small, the SAED pattern indicates that randomly oriented grains are obtained, and the calculated average grain size by XRD pattern is 39.22 nm. Furthermore, the XRD pattern indicates that the diffraction peak only becomes wider and no new diffraction peak is observed after CEPUT compared with Fig. 3, which indicates that the tool contamination is ignorable, especially on the top surface. This finding could be primarily attributed to the short contact time and the cooling temperature which inhibit the interdiffusion of elements between the tool and the processed material. In Ref. [39], the average grain size for the cryogenic SMAT copper sample is approximately 135 nm, which is approximately 60% smaller than that for SMAT copper sample at room temperature. Therefore, CEPUT is superior to typical SMAT process. Fig. 6 C-E and G-I show the grain color maps and the corresponding grain size distribution in the different outlined regions by white line in A. Specifically, Fig. 6C shows the grain color map of the region with 5-20 μm depth from the top surface outlined by white line in A, and Fig. 6G shows the corresponding grain size distribution. Fig. 6D shows the grain color map of the region with 50 - 100 μm depth from the top surface outlined by white line in A, and Fig. 6H shows the corresponding grain size distribution. Fig. 6E shows the grain color map of the region with 200 - 400 μm depth from the top surface outlined by white line in A, and Fig. 6I shows the corresponding grain size distribution. As shown in Fig. 6 C-E and G-I, the grain size gradually increases with the increase of the depth from the top surface after CEPUT. Moreover, the grain shapes are obviously different at different depths from the top surface. The grains at 5 - 20 μm depth (Fig. 6C) are fine and uniform, the grains at 50 - 100 μm depth (Fig. 6D) are elongated and nearly parallel to the treated surface, and the grains at 200 - 400 μm depth (Fig. 6E) are large and inhomogeneous. The phenomena can be explained as follows. The severity of plastic deformation produced by coupling the micro thermal shock from high peak pulse current and the micro mechanical shock from ultrasonics decreases with the increase of the depth from the treated surface. The acted force, heat, and the deformation of grains at 200 - 400 μm depth are small. Thus, the grains at 200 - 400 μm depth are large and inhomogeneous. The acted force and heat increase and the force is tangential to the treated surface due to the tool tip movement during CEPUT with the decrease of the depth from the treated surface. Thus, the grains at 50 - 100 μm depth are elongated and nearly parallel to the treated surface. However, SPD is produced, and the grains at 5 - 20 μm depth are refined with the decrease of the depth from the treated surface. Thus, the grains are fine and uniform.

To investigate the beneficial effect of CEPUT in terms of the effective depth and grain size of GN layer, the research on ultrasonic treatment only is conducted with the same ultrasonic parameters. The results are shown in Fig. 7. As shown in this figure, a similar microstructure is observed with ultrasonic treatment only like that with CEPUT. However, the average grain size on the top surface treated with CEPUT (39.22 nm) is approximately 60% smaller than that with ultrasonic treatment only (88.18 nm). Meanwhile, a smaller grain is obtained with CEPUT at the same depth from the treated surface compared with ultrasonic treatment only, which indicates that CEPUT can both refine the surface grain and increase the deformation layer thickness with the same ultrasonic parameters. Moreover, with the proper combination of the ultrasonic treatment parameters or the proper combination of the CEPUT parameters, the finer grain structures will be produced. Fig. 8 shows the time evolution of the microstructure and rearrangements of dislocation structures induced by SPD for the CEPUT sample, which are used to explain the aforementioned phenomena. Fig. 8A shows the original coarse grains before CEPUT. During the initiation of CEPUT, the heat from the high peak current and the force from the ultrasonic vibration both act on the original coarse grains, and several dislocations randomly occur in original coarse grains, as shown in Fig. 8B. In Ref. [27], Sprecher et al. investigated the effects of high-density current pulses on the flow stress of various polycrystalline metals at 300 K. They determined that the plastic strain contribution on the load was caused by the enhancement of dislocation mobility due to the action of drift electrons. Moreover, the electron wind "push" coefficient Bew was determined for Al and Cu and was confirmed in the order of 10^{-4} dyn s/cm^2 , which was in accordance with Roschupkin et al.'s theory. On the basis of the above research, the equivalent stress of the heat and the force significantly increases, the grain deformation resistance significantly decreases due to the large electron-windforce, and the stress and the strain both increase with the increase of time during CEPUT, which make the quantity of dislocations in the grain rapidly increase, and the high density dislocations are produced in the grains, as shown in Fig. 8C. The dislocation wall is formed by the high-density dislocation in the grain and evolves into the sub-grain boundaries, and the high angle grain boundary divides the original large grain into small grains with the increase of plastic deformation, as shown in Fig. 8D. After the sufficient passes of CEPUT treatment, a new dislocation wall is formed in the refined grain, a nanoscale dislocation wall is produced, and nanocrystals are generated eventually, as shown in Fig. 8E. The time evolution of the sample microstructure during CEPUT is also confirmed by the grain boundary distribution and misorientation angle at different depths from the top surface, shown in Fig. 9. Fig. 9A and B shows the grain boundary distribution and misorientation angle of the region with 200 - 400 μm depth from the top surface, which can be considered as the early stage of the plastic deformation during CEPUT. The dislocations are generated and then slip due to the high-strain-rate effects. By the coupling of thermal and athermal effects of electropulsing, a large flux of atoms is produced, the dislocation climbing is accelerated, and the piledup dislocations are rearranged by cross-slip, climb and annihilation [31-33]. Therefore, the density of dislocations is decreased near the grain boundaries, the sub-boundary with low angle misorientation is produced, and the fraction of low angle grain boundary (LAGB) is only 35.2%. In this study, the grain boundary with the misorientation between 2° and 15° is considered as the low angle grain boundary, and the grain boundary with the misorientation higher than 15° is considered as the high angle grain boundary (HAGB). As the depth from the top surface decreases, which can be considered that the time increases during CEPUT, as shown in Fig. 9C and D, the stress and the strain both increase, which results in the increase of the grain deformation and the dislocation density. Thus, the number of LAGB increases. As the time increases further, the dislocation density reaches to a critical value, many dislocations are annihilated and rearranged near the sub-boundary, the misorientation between both sides of the grain boundaries increases, and LAGB evolves into HAGB, which results in the increase of HAGB and divides the original coarse grain into many small grains (Fig. 9E and F). Moreover, as shown in Fig. 10, the maximum stress, and the maximum temperature are all generated at the contact point, and the variance of the two parameters at the contact point are all large during CEPUT. The dislocation density is so high that the nanoscale dislocation wall is produced (Fig. 11), and nanocrystals are easily generated. From another point of view, the drift electrons push the dislocations when high density electric pulse passes through the sample during CEPUT, which lower the dislocation density, enhance the dislocation mobility, and accelerate atom diffusion and reconstruction, increase the nucleation rate of recrystallization, and lower the energy obstacle in thermodynamically driving these processes [30,40]. On the other hand, the ultrafast and focused energy input by high density electric pulse and ultrasonic shock is facilitated in the strain-induced recrystallization, which positively decreases the required recrystallization temperature [41,42]. Moreover, the temperature at the contact point region rapidly increases, and dynamic recrystallization occurs in the sample. Therefore, dynamic recrystallization occurs, which is positive for grain refinement in CEPUT. The output load-displacement curves for the treated specimen with CEPUT is given in Fig. 12A. Apparently, all the curves present a parabolic shape in the loading stage and a horizontal straight line in the load holding stage. After unloading, the indentation depth is slightly reduced for all the cases due to material elastic recovery. Moreover, the maximum displacement and residual displacement decrease when the indentation location becomes close to the treated surface, which indicates that the strengthening effect tends to be obvious with the reduction of surface distance, as shown in Fig. 12B. Moreover, as shown in Fig. 12B, the surface hardness after CEPUT reaches 2.105 GPa, and the hardness decreases with the depth increasing. The continuous decrease of hardness with an increasing depth is consistent with the increase in grain size. Furthermore, it can also be seen from Fig. 12B that the hardness is nearly constant for the distance from 200 μm to 600 μm from the treated surface. The reason for that may be the multifactor function of the acoustic softening effect, the refined grain, the plastic strain, and the increased piled-up dislocations in that region during CEPUT. As depicted in Fig. 12C and D, the maximum texture intensity of the base material and the sample surface after CEPUT are 6.130 and 2.003, respectively, which indicates that the treated sample surface tends to be isotropic. The reason for this is that many randomly oriented small grains and nanocrystals are generated on the treated surface during CEPUT. Thus, CEPUT can reduce the texture on the sample surface aside from grain refinement, which is favorable for the CEPUT application.

Conclusion

A new efficient method by coupling the micro thermal shock from high peak pulse current and the micro mechanical shock from ultrasonics for the preparation of the GN on the metal surface is developed using CEPUT. In this method, the grain increases and the hardness decreases with the depth from the top surface increasing, and the texture in the original sample is reduced. Moreover, the average surface grain size decreases from 48.77 μm to 39.22 nm, the hardness reaches to 2.105 GPa, and the thickness of the SPD layer reaches to approximately 500 mm after CEPUT. Furthermore, a computational model is developed and the grain refinement mechanism is proposed to describe the electrical-thermalmechanical phenomena during CEPUT. This simple and costeffective method, which will find potential applications in a wide range of industrial processes, is effective, especially on metals with high thermal and electrical conductivity. CEPUT provides a rapid and highly efficient method for the introduction of a GN at the surface of metal samples in fundamental and applied interest. CEPUT effects really consists of contact stress effect and thermal effect (joule heating) with electroplastic effect such as electronwind-force. However, we did not separate their contribution to grain refinement and effective depth quantificationally in this paper, and these works will be done in the future.

Author contributions

Renjie Ji, Yonghong Liu and Suet To equally contributed to the idea. Renjie Ji, Zelin Yang and Hui Jin performed the experiments, and characterized the microstructure of the treated sample with EBSD and TEM. Baoping Cai and Chao Zheng developed the physical and mathematical model of CEPUT. Wai Sze Yip performed the composition analysis. Renjie Ji and Yonghong Liu wrote the paper. Chao Zheng, Zelin Yang and Hui Jin edited the figures.

Completing Interests

The authors declare that they have no competing interests.

Acknowledgments

This work was supported by the National Natural Science Foundation of China (Grant No. 51675535), China Postdoctoral Science Foundation (Grant No. 2015M570619), Key Pre-Research Foundation of Military Equipment of China (Grant No. 6140923030702), and the Fundamental Research Funds for Central Universities (Grant No. 15CX08007A, 17CX02058).

References

[1] K.A. Darling, M. Rajagopalan, M. Komarasamy, M.A. Bhatia, B.C. Hornbuckle, R.S. Mishra, K.N. Solanki, Extreme creep resistance in a microstructurally stable nanocrystalline alloy, Nature 537 (2016) 378-381.

[2] K. Lu, L. Lu, S. Suresh, Strengthening materials by engineering coherent internal boundaries at the nanoscale, Science 324 (2009) 349-352.

[3] H. Kou, J. Lu, Y. Li, High-strength and high-ductility nanostructured and amorphous metallic materials, Adv. Mater. 26 (2014) 5518-5524.

[4] K. Lu, Making strong nanomaterials ductile with gradients, Science 345 (2014) 1455-1456.

[5] T.H. Fang, W.L. Li, N.R. Tao, K. Lu, Revealing extraordinary intrinsic tensile plasticity in gradient nano-grained copper, Science 331 (2011) 1587-1590.

[6] X.C. Liu, H.W. Zhang, K. Lu, Strain-induced ultrahard and ultrastable nanolaminated structure in nickel, Science 342 (2013) 337-340.

[7] Z. Ni, X. Wang, J. Wang, E. Wu, Characterization of the phase transformation in a nanostructured surface layer of 304 stainless steel induced by high-energy shot peening, Physica B 334 (2003) 221-228.

[8] L. Zhang, A. Ma, J. Jiang, D. Song, D. Yang, J. Chen, Electrochemical corrosion properties of the surface layer produced by supersonic fine-particles bombarding on low-carbon steel, Surf. Coating. Technol. 232 (2013) 412-418.

[9] K.A. Darling, M.A. Tschopp, A.J. Roberts, J.P. Ligda, L.J. Kecskes, Enhancing grain refinement in polycrystalline materials using surface mechanical attrition treatment at cryogenic temperatures, Scr. Mater. 69 (2013) 461-464.

[10] Y. Wei, J. Liu, H. Wang, H. Gao, Evading the strength-ductility trade-off dilemma in steel through gradient hierarchical nanotwins, Nat. Commun. 5 (2014) 3580.

[11] S.Q. Deng, A. Godfrey, W. Liu, N. Hansen, A gradient nanostructure generated in pure copper by platen friction sliding deformation, Scr. Mater. 117 (2016) 41-45.

[12] X. Yuan, Y. Sun, C. Li, W. Liu, Experimental investigation into the effect of low plasticity burnishing parameters on the surface integrity of TA2, Int. J. Adv. Manuf. Technol. 88 (2017) 1089-1099.

[13] A. Marcon, S.N. Melkote, M. Yoda, Effect of nozzle size scaling in co-flow water cavitation jet peening, J. Manuf. Process. 31 (2018) 372-381.

[14] L. Shi, C.S. Wu, G.K. Padhy, S. Gao, Numerical simulation of ultrasonic field and its acoustoplastic influence on friction stir welding, Mater. Des. 104 (2016) 102-115.

[15] Z. Yao, G.Y. Kim, Z. Wang, L.A. Faidley, Q. Zou, D. Mei, Z. Chen, Acoustic softening and residual hardening in aluminum: modeling and experiments, Int. J. Plast. 39 (2012) 75-87.

[16] Y. Long, Y. Li, J. Sun, I. Ille, J. Li, J. Twiefel, Effects of process parameters on force reduction and temperature variation during ultrasonic assisted incremental sheet forming process, Int. J. Adv. Manuf. Technol. (2018). https://doi.org/10.1007/s00170-018-1886-0.

[17] Y. Liu, S. Suslov, Q. Han, L. Hua, C. Xu, Comparison between ultrasonic vibration-assisted upsetting and conventional upsetting, Metall. Mater. Trans. 44 (2013) 3232-3244.

[18] F. Djavanroodi, H. Ahmadian, R. Naseri, K. Koohkan, M. Ebrahimi, Experimental investigation of ultrasonic assisted equal channel angular pressing process, Arch. Civ. Mech. Eng. 16 (2016) 249-255.

[19] S. Bagherzadeh, K. Abrinia, Q. Han, Ultrasonic assisted equal channel angular extrusion (UAE) as a novel hybrid method for continuous production of ultrafine grained metals, Mater. Lett. 169 (2016) 90-94.

[20] A. Amanov, Y.S. Pyun, Lowering friction of ball screws made of different steel grades through ultrasonic impact treatment, Tribol. Int. 123 (2018) 105-119.

[21] YuN. Petrov, G.I. Prokopenko, B.N. Mordyuk, M.A. Vasylyev, S.M. Voloshko, V.S. Skorodzievski, V.S. Filatova, Influence of microstructural modifications induced by ultrasonic impact treatment on hardening and corrosion behavior of wrought Co-Cr-Mo biomedical alloy, Mater. Sci. Eng. C 58 (2016) 1024-1035.

[22] Y. Liu, X. Zhao, D. Wang, Determination of the plastic properties of materials treated by ultrasonic surface rolling process through instrumented indentation, Mat. Sci. Eng. A-Struc. 600 (2014) 21-31.

[23] M. Kheradmandfard, S.F. Kashani-Bozorg, C.L. Kim, A.Z. Hanzaki, Y.S. Pyoun, J.H. Kim, A. Amanov, D.E. Kim, Nanostructured b-type titanium alloy fabricated by ultrasonic nanocrystal surface modification, Ultrason. Sonochem. 39 (2017) 698-706.

[24] L. Zhou, Y. Li, W. He, G. He, X. Nie, D. Chen, Z. Lai, Z. An, Deforming TC6 titanium alloys at ultrahigh strain rates during multiple laser shock peening, Mat. Sci. Eng. A-Struc. 578 (2013) 181-186.

[25] S. Lou, Y. Li, L. Zhou, X. Nie, G. He, Y. Li, W. He, Surface nanocrystallization of metallic alloys with different stacking fault energy induced by laser shock processing, Mater. Des. 104 (2016) 320-326.

[26] O.A. Troitskii, Electromechanical effect in metals, JETP Lett. (Engl. Transl.) 10 (1969) 11-14.

[27] A.F. Sprecher, S.L. Mannan, H. Conrad, On the mechanisms for the electroplastic effect in metals, Acta Metall. 34 (1986) 1145-1162.

[28] M.I. Molotskii, Theoretical basis for electro- and magnetoplasticity, Mater. Sci. Eng. A 287 (2000) 248-258.

[29] O.A. Troitskiy, Y.A. Perlovich, V.N. Sikorov, B.A. Kruglov, A.L. Kostyshev, Y.V. Nikitenko, I.A. Lipyanko, M.G. Isayenkova, Features of texture formation in copper during electroplastic rolling, Phys. Met. Metallogr. 71 (1991) 176-180.

[30] X. Ye, T. Liu, Y. Ye, H. Wang, G. Tang, G. Song, Enhanced grain refinement and microhardness of Ti-Al-V alloy by electropulsing ultrasonic shock, J. Alloys Compd. 621 (2015) 66-70.

[31] D. Li, E. Yu, Computation method of metal's flow stress for electroplastic effect, Mater. Sci. Eng. A 505 (2009) 62-64.

[32] J. Kuang, X. Du, X. Li, Y. Yang, A.A. Luo, G. Tang, Athermal influence of pulsed electric current on the twinning behavior of Mg-3Al-1Zn alloy during rolling, Scr. Mater. 114 (2016) 151-155.

[33] H. Wang, G. Song, G. Tang, Evolution of surface mechanical properties and microstructure of Ti-6Al-4V alloy induced by electropulsing-assisted ultrasonic surface rolling process, J. Alloys Compd. 681 (2016) 146-156.

[34] X. Li, G. Tang, J. Kuang, X. Li, J. Zhu, Effect of current frequency on the mechanical properties, microstructure and texture evolution in AZ31 magnesium alloy strips during electroplastic rolling, Mat. Sci. Eng. A-Struc. 612 (2014) 406-413.

[35] B. Kinsey, G. Cullen, A. Jordan, S. Mates, Investigation of electroplastic effect at high deformation rates for 304SS and Ti-6Al-4V, CIRP Ann. Manuf. Technol. 62 (2013) 279-282.

[36] J. Shen, Y. Zhang, X. Lai, P.C. Wang, Modeling of resistance spot welding of multiple stacks of steel sheets, Mater. Des. 32 (2011) 550-560.

[37] N. Ma, H. Murakawa, Numerical and experimental study on nugget formation in resistance spot welding for three pieces of high strength steel sheets, J. Mater. Process. Technol. 210 (2010) 2045-2052.

[38] H. Moshayedi, I. Sattari-Far, Numerical and experimental study of nugget size growth in resistance spot welding of austenitic stainless steels, J. Mater. Process. Technol. 212 (2012) 347-354.

[39] K.A. Darling, M.A. Tschopp, A.J. Roberts, J.P. Ligda, L.J. Kecskes, Enhancing grain refinement in polycrystalline materials using surface mechanical attrition treatment at cryogenic temperatures, Scr. Mater. 69 (2013) 461-464.

[40] C. Xu, Y. Li, X. Rao, Effect of electropulsing rolling on mechanical properties and microstructure of AZ31 magnesium alloy, Trans. Nonferrous Metals Soc. China 24 (2014) 3777-3784.

[41] Q. Xu, L. Guan, Y. Jiang, G. Tang, S. Wang, Improved plasticity of Mg-Al-Zn alloy by electropulsing tension, Mater. Lett. 64 (2010) 1085-1087.

[42] Q. Xu, G. Tang, Y. Jiang, Thermal and electromigration effects of electropulsing on dynamic recrystallization in Mg-3Al-1Zn alloy, Mater. Sci. Eng. A 528 (2011) 4431-4436.

Table 1 The distance of the test point from the treated workpiece top surface.

Test point list	1	2	3	4	5	6	7	8
Distance of test point from top surface (μm)	30	60	90	120	150	200	400	600

Table 2 Material properties of the workpiece and the treatment tool.

	Copper	Cemented carbide
Density (kg/m^3)	8.93 x 10^3	12.90 x 10^3
Thermal expansion coefficient (K^{-1})	1.7 x 10^{-5}	6 x 10^{-6}
Heat conductivity (W/m K)	388	110
Specific heat (J/kg K)	395	950
Yield strength (MPa)	70.1	946

Elastic modulus (GPa)	110	710
Poisson's ratio	0.34	0.19

Fig. 1. Physical model and experimental device for CEPUT. (A) Physical model, (B) Pulse current waveform, (C) Experimental device.

Fig. 2. Grain color map and grain size distribution of copper sample. (For interpretation of the references to color in this figure legend, the reader is referred to the Web version of this article.)

Fig. 3. XRD pattern of the copper sample.

Fig. 4. Geometrical model for CEPUT.

Fig. 5. Simulation procedure for CEPUT process.

Fig. 6. Microstructure of copper sample section after CEPUT. (A) The microstructural transition in the top 700 μm of the treated sample, (B) TEM bright field image, and the corresponding SAED pattern of the top surface indicated in A, (C), (D), (E) the grain color maps at the different regions outlined by white line in A, (F) XRD pattern of the top surface indicated in A, (G), (H), (I) the corresponding grain size distribution of (C), (D), (E), respectively. (For interpretation of the references to color in this figure legend, the reader is referred to the Web version of this article.)

Fig. 7. Microstructure of copper sample section after ultrasonic treatment only. (A) The microstructural transition in the top 700 μm of the treated sample, (B) TEM

bright field image, and the corresponding SAED pattern of the top surface indicated in A, (C), (D), (E) the grain color maps at the different regions outlined by white line in A, (F) XRD pattern of the top surface indicated in A, (G), (H), (I) the corresponding grain size distribution of (C), (D), (E), respectively. (For interpretation of the references to color in this figure legend, the reader is referred to the Web version of this article.)

Fig. 8. Microstructure evolution and rearrangements of dislocation structures induced by SPD during CEPUT. (A) The original coarse grains, (B) low density dislocations produced randomly at SPD early stage, (C) high density dislocations produced in the grains, (D) sub-grain boundaries produced to divide the original coarse grain into small grains, (E) nanocrystal grains produced by many passes treatment.

Fig. 9. The distribution of grain boundary and misorientation angle of the sample treated with CEPUT. Grain boundary distributions of the region of (A) 200 - 400 µm, (C) 50 - 100 µm, (E) 5 - 20 µm, depth from the top surface, respectively. Misorientation angle distributions of the region of (B) 200 - 400 µm, (D) 50 - 100 µm, (F) 5 - 20 µm, depth from the top surface, respectively

Fig. 10. FEM simulation results during CEPUT. (A) Contact stress distribution at the contact point region, (B) the variance of the contact stress at the contact point, (C) temperature field at the contact point region, (D) the variance of the temperature at the contact point.

Fig. 11. Dislocation distribution in the top surface after CEPUT [red dashed zone indicates dislocations with high density]. (For interpretation of the references to color in this figure legend, the reader is referred to the Web version of this article.)

Fig. 12. Performance of copper sample treated with CEPUT. (A) Load-displacement responses for treated specimen, (B) nanohardness distribution of treated copper section, (C) and (D) pole figures of treated sample section of the region shown in Fig. 6C and base material shown in Fig. 2, respectively.

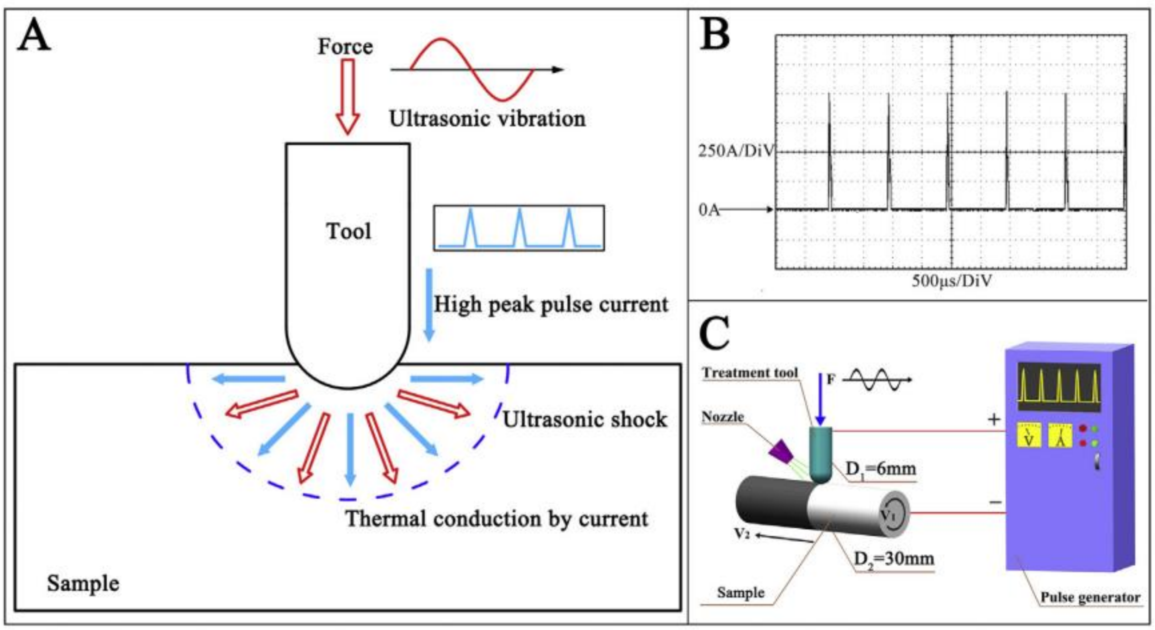

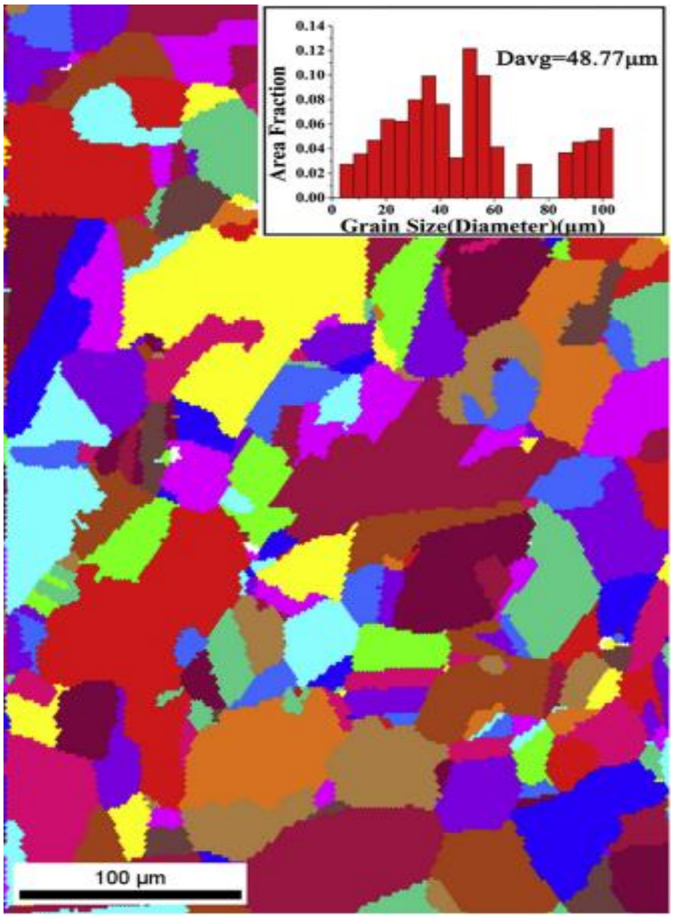
Davg=48.77μm
Area Fraction
Grain Size(Diameter)(μm)
100 μm

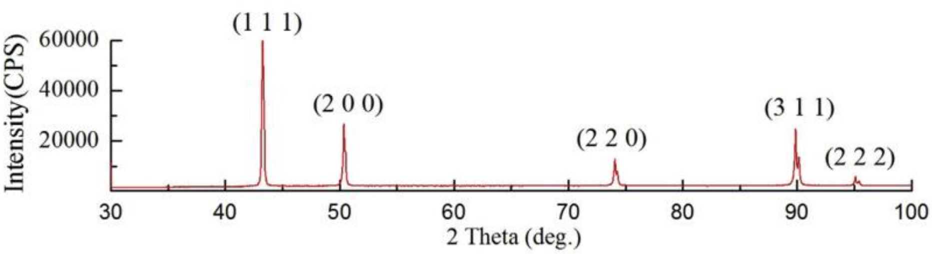
(1 1 1)
(2 0 0)
(2 2 0)
(3 1 1)
(2 2 2)
Intensity(CPS)
2 Theta (deg.)

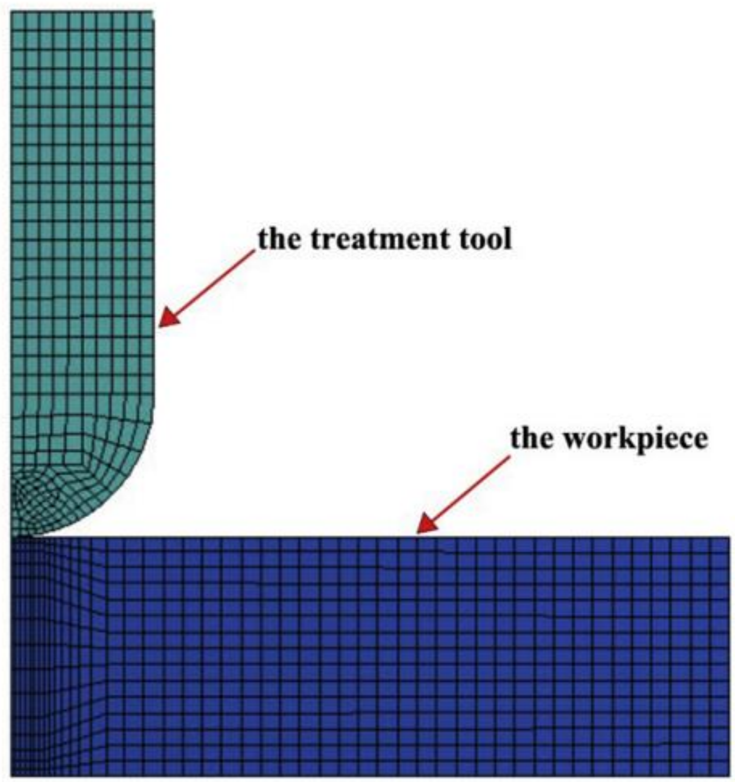
the treatment tool
the workpiece

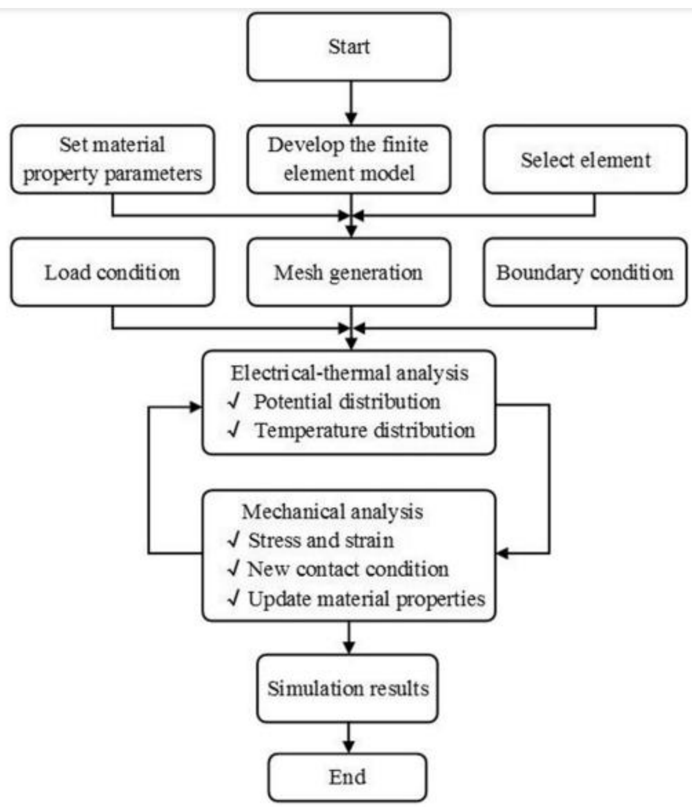
Start
Set material property parameters
Develop the finite element model
Select element
Load condition
Mesh generation
Boundary condition
Electrical-thermal analysis
√ Potential distribution
√ Temperature distribution
Mechanical analysis
√ Stress and strain
√ New contact condition
√ Update material properties
Simulation results
End

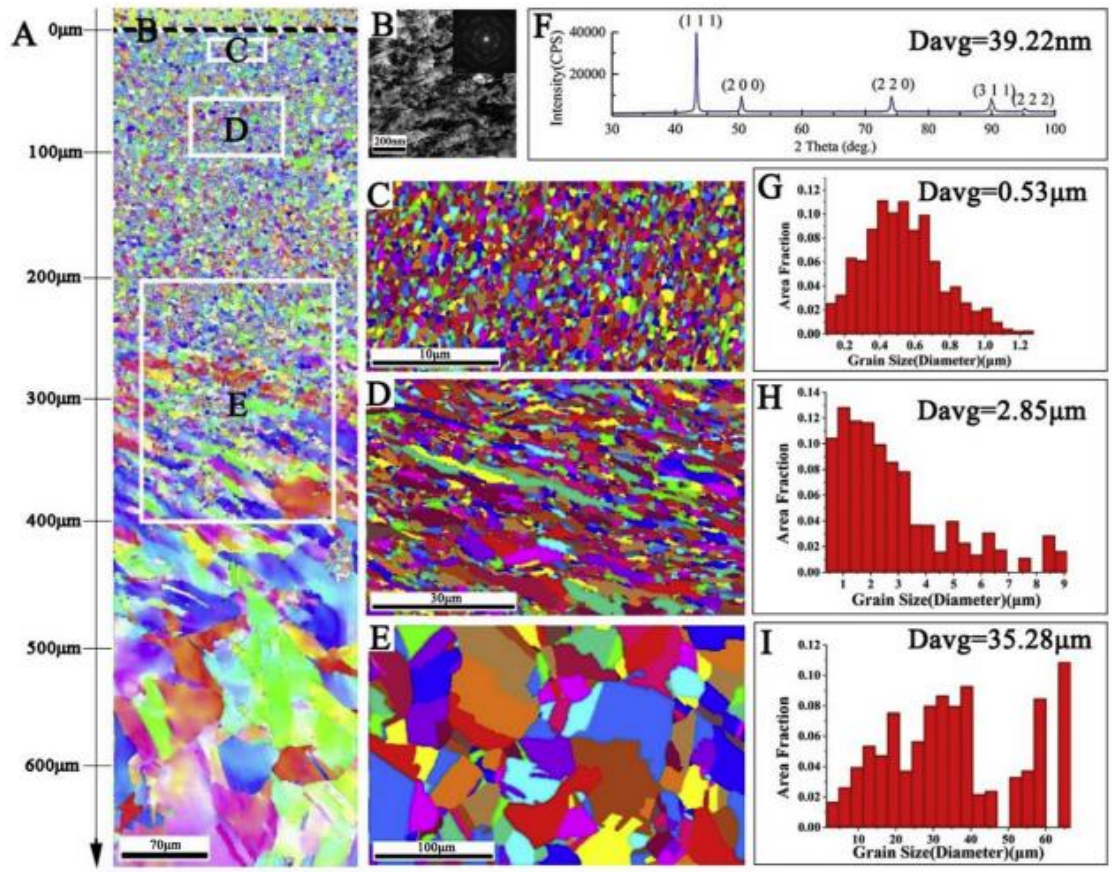
A
0μm
100μm
200μm
300μm
400μm
500μm
600μm
B
C
D
E
70μm
B
200nm
F
(1 1 1)
Davg=39.22nm
40000
20000
Intensity(CPS)
(2 0 0)
(2 2 0)
(3 1 1)
(2 2 2)
30 40 50 60 70 80 90 100
2 Theta (deg.)
C
10μm
G
Davg=0.53μm
Area Fraction
Grain Size(Diameter)(μm)
D
30μm
H
Davg=2.85μm
Area Fraction
Grain Size(Diameter)(μm)
E
100μm
I
Davg=35.28μm
Area Fraction
Grain Size(Diameter)(μm)

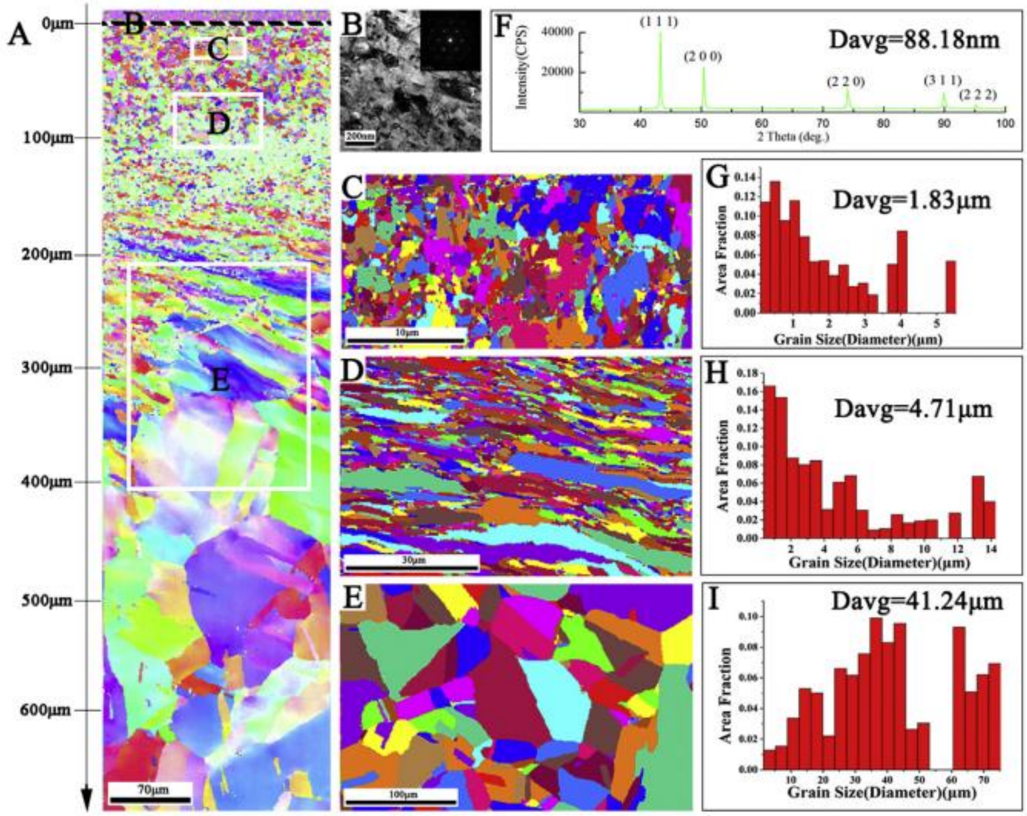
A
0μm
100μm
200μm
300μm
400μm
500μm
600μm
B
C
D
E
70μm
200nm
F
Davg=88.18nm
Intensity(CPS)
40000
20000
(1 1 1)
(2 0 0)
(2 2 0)
(3 1 1)
(2 2 2)
2 Theta (deg.)
10μm
G
Davg=1.83μm
Area Fraction
Grain Size(Diameter)(μm)
30μm
H
Davg=4.71μm
100μm
I
Davg=41.24μm

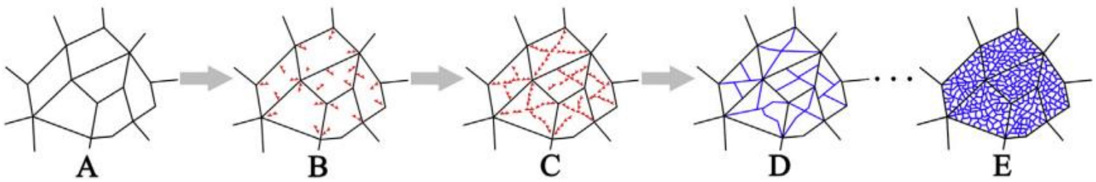

A
B
C
D
E

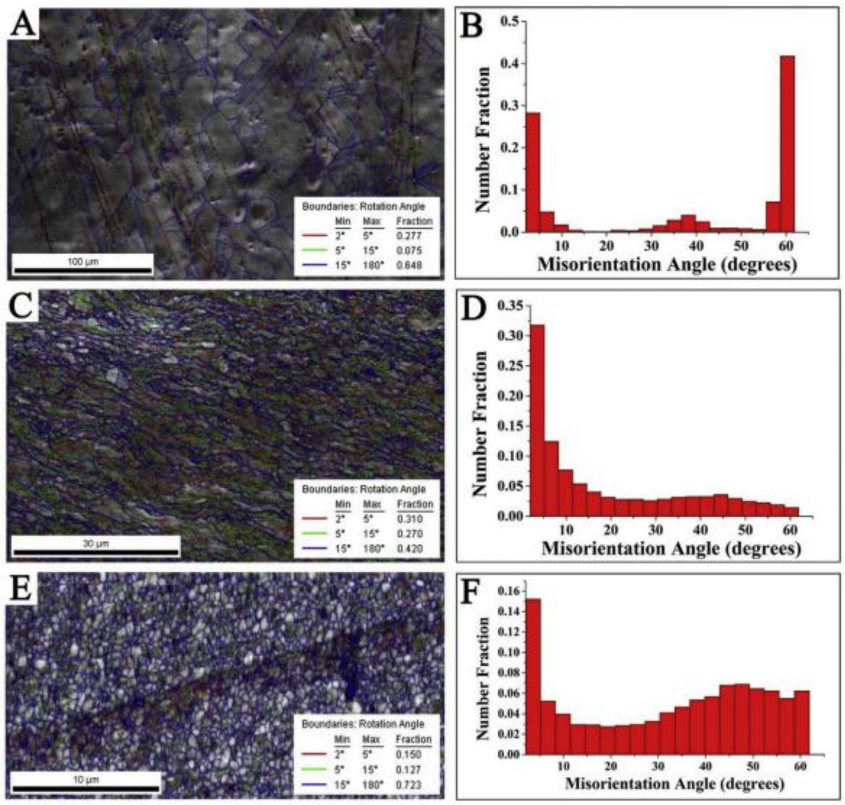

A
Boundaries: Rotation Angle
Min Max Fraction
2° 5° 0.277
5° 15° 0.075
15° 180° 0.648
100 µm
B
Number Fraction
Misorientation Angle (degrees)
C
Boundaries: Rotation Angle
Min Max Fraction
2° 5° 0.310
5° 15° 0.270
15° 180° 0.420
30 µm
D
Number Fraction
Misorientation Angle (degrees)
E
Boundaries: Rotation Angle
Min Max Fraction
2° 5° 0.150
5° 15° 0.127
15° 180° 0.723
10 µm
F
Number Fraction
Misorientation Angle (degrees)

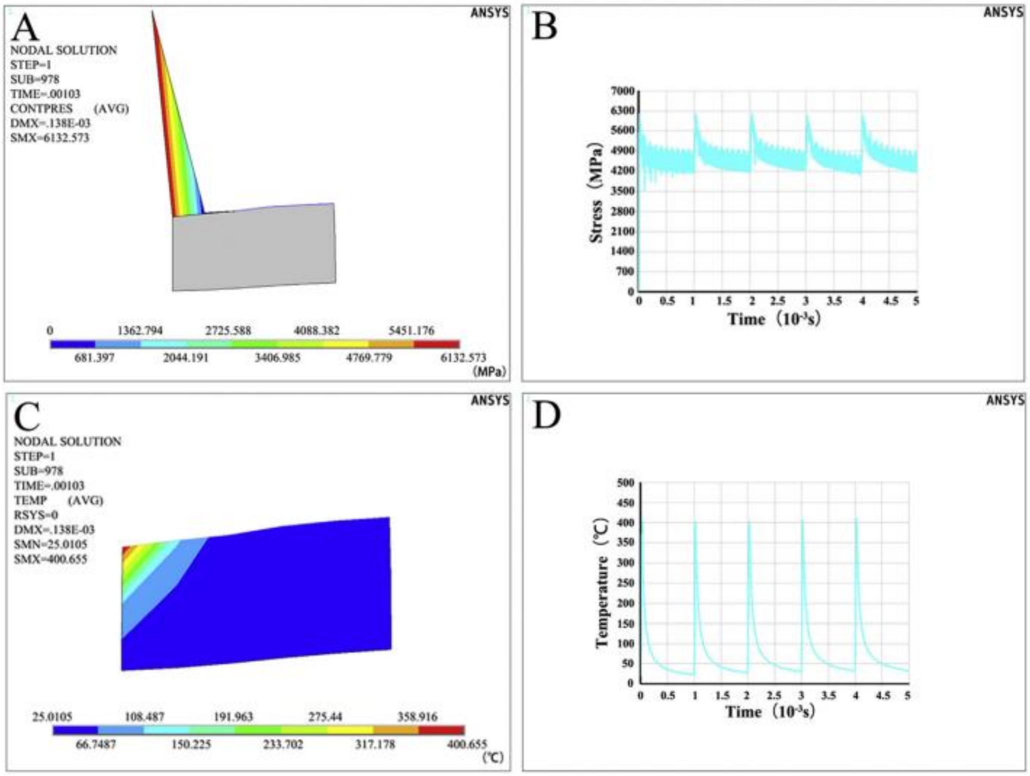
A
ANSYS
NODAL SOLUTION
STEP=1
SUB=978
TIME=.00103
CONTPRES (AVG)
DMX=.138E-03
SMX=6132.573
0
1362.794
2725.588
4088.382
5451.176
681.397
2044.191
3406.985
4769.779
6132.573
(MPa)
B
ANSYS
Stress（MPa）
Time（10^{-3}s）
C
ANSYS
NODAL SOLUTION
STEP=1
SUB=978
TIME=.00103
TEMP (AVG)
RSYS=0
DMX=.138E-03
SMN=25.0105
SMX=400.655
25.0105
108.487
191.963
275.44
358.916
66.7487
150.225
233.702
317.178
400.655
(℃)
D
ANSYS
Temperature（℃）
Time（10^{-3}s）

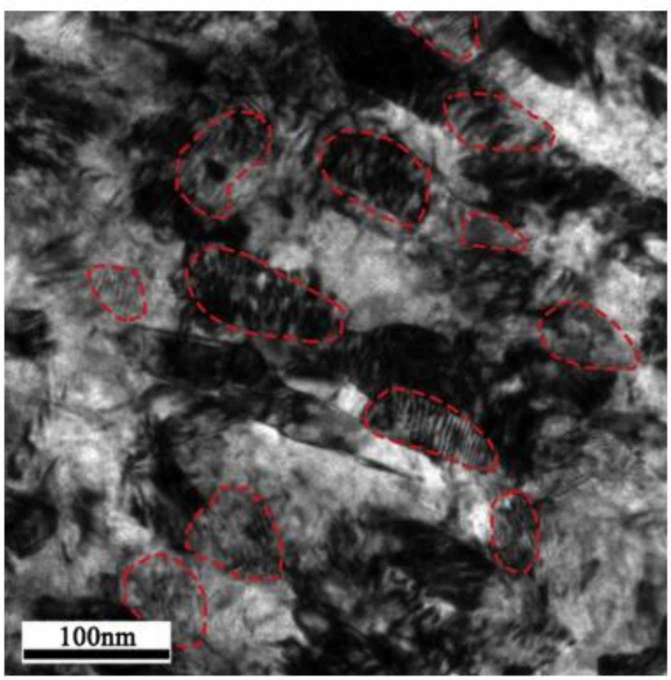
100nm

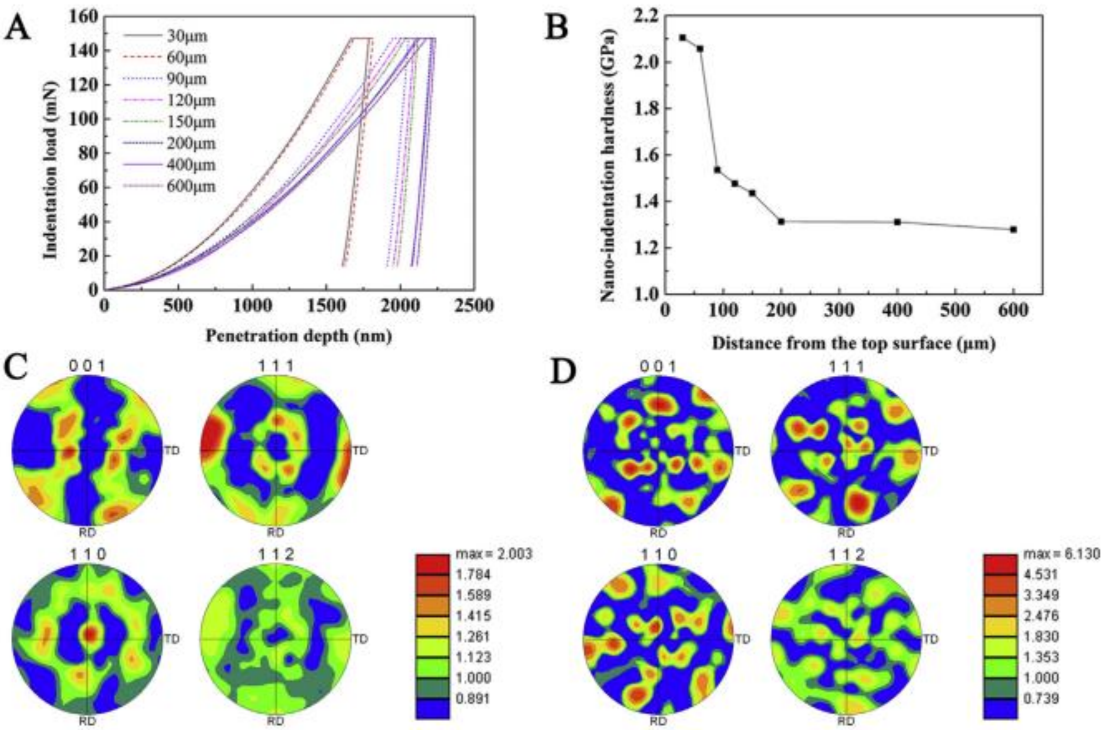

A
Indentation load (mN)
Penetration depth (nm)
30μm
60μm
90μm
120μm
150μm
200μm
400μm
600μm
B
Nano-indentation hardness (GPa)
Distance from the top surface (μm)
C
0 0 1
1 1 1
1 1 0
1 1 2
TD
RD
max = 2.003
1.784
1.589
1.415
1.261
1.123
1.000
0.891
D
max = 6.130
4.531
3.349
2.476
1.830
1.353
1.000
0.739